Available online at www.sciencedirect.com
ScienceDirect
Acta Materialia 59 (2011) 5627–5637
Acta MATERIALIA
www.elsevier.com/locate/actamat

Emergence of strain-rate sensitivity in Cu nanopillars: Transition from dislocation multiplication to dislocation nucleation

Andrew T. Jennings [a,*], Ju Li [b], Julia R. Greer [a]

[a] Division of Engineering and Applied Science, California Institute of Technology, 1200 E. California Blvd., Pasadena, CA 91125, USA
[b] Department of Materials Science and Engineering, University of Pennsylvania, Philadelphia, PA 19104, USA

Received 13 January 2011; received in revised form 13 May 2011; accepted 20 May 2011
Available online 21 June 2011

Abstract

We demonstrate strain-rate sensitivity emerging in single-crystalline Cu nanopillars with diameters ranging from 75 up to 500 nm through uniaxial deformation experiments performed at different constant strain rates. In the range of pillar diameters and strain rates tested, we find that the size dependence of the pillar strength deviates from the ubiquitously observed power law to a relatively size-independent flow strength, markedly below the predicted theoretical strength for strain rates slower than 10^{-1} s^{-1}. We find this transition diameter, D_t, to be a function of strain rate, where faster strain rates shift the transition diameter to smaller pillar diameters: $D_t \sim 150$ nm at 10^{-3} s^{-1} and $D_t \sim \leqslant 75$ nm at 10^{-1} s^{-1}. We compute the activation volumes, Ω, as a function of pillar diameter at each strain rate and find that for pillar diameters below D_t, the activation volumes are relatively small, $\Omega < 10b^3$. This range agrees favorably with atomistic simulations for dislocation nucleation from a free surface. We postulate a plasticity mechanism transition from dislocation multiplication via the operation of truncated dislocation sources, also referred to as single-arm sources, in pillars with diameters greater than D_t to dislocation nucleation from the surface in the smaller samples.

Keywords: Nanostructure; Copper; Theory; Compression test

1. Introduction

A major current focus in the nanomechanical community is the investigation of single-crystalline strength at reduced dimensions through uniaxial deformation of cylindrical specimens, often referred to as micro- or nanopillars [1–5]. Remarkably, the results of all such experiments on face-centered cubic (fcc) crystals with non-zero initial dislocation densities indicate that their strengths depend on pillar diameter in a power-law fashion: $\sigma \propto D^{-n}$, where σ is the flow stress and D is the pillar diameter, with $0.5 \leqslant n \leqslant 1.0$ [1–5]. Size-dependent strength is counter-intuitive, as crystalline strength in bulk is generally considered to be independent of sample size. In bulk metals, strength is proportional to the increasing-with-strain dislocation density via the Taylor relation: $\sigma \propto \mu b\sqrt{\rho}$ [6], whereby dislocations multiply via double-cross slip and by operation of pinned dislocation sources [7].

Recent modeling efforts have probed possible types of dislocation sources in pillars at a range of length scales from ~1 nm up to several microns. For example, dislocation dynamics (DD) simulations performed on micron-sized pillars reveal that in these relatively large samples, single-arm, or spiral, dislocation sources generate stochastic stress–strain signatures and unambiguous size effects, in accordance with those observed experimentally [8–13]. If the pillar dimensions are reduced by an order of magnitude, molecular dynamics (MD) simulations of nanowires then show the nucleation of partial dislocations from the surface of the wire [14–16]. An important consideration is that neither type of simulation has been able to accurately capture both mechanisms simultaneously: discrete DD

* Corresponding author. Tel.: +1 626 395 4416; fax: +1 626 395 8868.
E-mail address: jennings@caltech.edu (A.T. Jennings).

1359-6454/$36.00 © 2011 Acta Materialia Inc. Published by Elsevier Ltd. All rights reserved.
doi:10.1016/j.actamat.2011.05.038

simulations cannot accurately describe surface nucleation, whereas MD simulations are too computationally intensive to accurately describe the collective DD of large systems.

Major advances investigating in depth the crystalline plasticity in the sub-micron regime have also been enabled via *in situ* transmission electron microscopy (TEM) tensile tests. These experiments reveal two mechanisms for dislocation generation in small-scale crystals: (i) via spiral, or single-arm, sources (SASs), as is the case for ~455 nm single-crystalline Al under tensile loading [17]; and (ii) via partial dislocation nucleation from the surface, or surface sources (SS), as revealed during uniaxial tension of ~15 nm diameter Au nanowires by Zheng et al. [18,19]. In the former, the dislocations are multiplied as they are generated from an already existing pinned source, while in the latter individual dislocations are nucleated stochastically, from a distribution of surface locations.

Although the precise nature of either type of source is being vigorously pursued, a general agreement exists that in micron-sized fcc pillars the dislocations multiply and form complex intertwined networks through the operation of SASs, whereas nanosized pillars are characterized by virtually non-existent dislocation multiplication or storage, and deform via dislocation nucleation at the surface (via SSs), glide and subsequent annihilation at the free surfaces. However, despite this general agreement, the possible coexistence and/or transition between these two mechanisms, as well as their strength, geometry, stability and thermal nature remain important open questions.

A previously unexplored route in nanopillar experiments is to probe the presence of a particular type of dislocation source by computing the activation volumes required for their operation. For example, atomistic simulations have predicted SSs to have an activation volume of ~1–10b^3 which would result in a significant thermal contribution to the source's strength [20]. In contrast, a SAS, often represented as a truncated Frank–Read source (FRS), whose activation volume is relatively large, ~100–1000b^3, would make an almost negligible thermal contribution to its strength [7]. We hypothesize that this great difference in the activation volumes should manifest itself in vastly different strain-rate dependences between the two mechanisms, with SSs being more sensitive to strain rate than SASs [7,20].

In this work, we present compressive behavior of single-crystalline Cu nanopillars with diameters between 75 and 500 nm, fabricated without the use of a focused ion beam (FIB) and deformed at different constant strain rates spanning over ~4 orders of magnitude. The dependence of the flow stress on the strain rate is measured to determine the activation volumes for each strain rate and pillar diameter, which are then compared to theoretically determined activation volumes. Our experiments reveal a discontinuity in the measured strain-rate sensitivity and activation volume, suggesting a possible deformation mechanism transition from collective DD to surface dislocation nucleation [21].

2. Experimental

2.1. Sample preparation and resulting microstructure

Single crystalline Cu nanopillars were fabricated by electroplating Cu from a Cu(II) sulfate bath under an applied voltage. A schematic of the electroplating process can be seen in Fig. 1A. The cathode, shown in a zoomed-in image in A, is a Si wafer upon which a ~100 nm thick Au/Ti seed layer was deposited to serve as an electrical contact. The Au seed layer had a columnar grain structure with a ⟨1 1 1⟩ texture and an average grain width larger than all pillar diameters tested. A poly (methyl methacrylate)

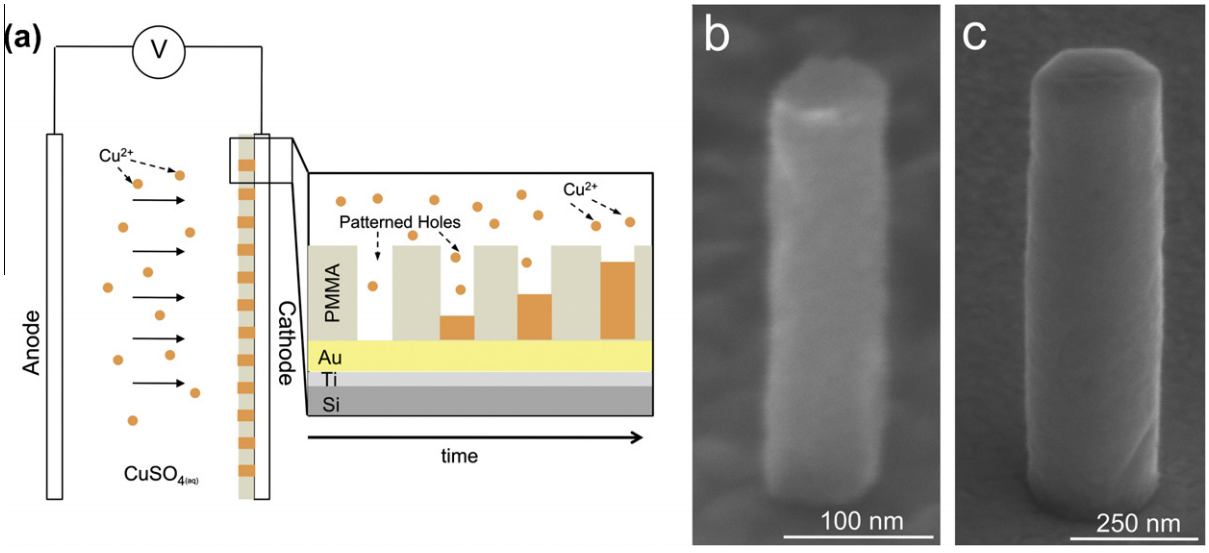

Fig. 1. (a) Schematic of the fabrication process. When a voltage is applied Cu^{2+} is reduced at the cathode. Details of the cathode structure show cylindrical holes patterned in a PMMA layer on top of a Au seed layer. Inset illustrates the holes progressively filling with Cu with increasing time. SEM images of 75 nm (b) and 500 nm (c) diameter Cu nanopillars fabricated by this technique.

(PMMA) layer was spun onto the seed layer; the PMMA was then patterned with cylindrical pores corresponding to the pillar diameter in an electron beam pattern generator (EBPG). This chip served as the cathode in the Cu bath described above. A voltage was applied between the insoluble anode and cathode, depositing Cu into the pores. Further details of the sample fabrication process can be found in Ref. [22]. Examples of typical 75 and 500 nm pillar morphologies are shown in Fig. 1B and C. These pillars had a loading axis oriented in $\sim\langle 1\,1\,1\rangle$ direction, and as a result of the electroplating process, they contained defects: initial dislocations and surface roughness. By the latter we mean that the surface was not atomically smooth or forcibly reorganized through sample preparation as in FIB pillar fabrication. Analysis of the surface roughness suggested a variation of ± 2 nm for each pillar diameter, resulting in an error in the recorded strength of $\pm 4\%$ for 100 nm pillars. TEM analysis of these copper electroplated pillars provided estimates of the dislocation density of $\sim 10^{14}\ \mathrm{m}^{-2}$, similar to other pillars produced by the FIB [23]. Most pillars tested had no taper; however, all pillars tested had less than 1° of vertical taper.

2.2. Mechanical testing

Pillars suitable for compression were identified by scanning electron microscopy (SEM), using an FEI Nova 200 microscope fitted with a gas injection system needle of $W(CO)_6$. Inside the microscope, a W annulus with an inner diameter of 6–8 μm and width of 1 μm was deposited at 52° tilt around each compression pillar in order to identify these pillars in the nanoindenter's optical system. Compression tests for five different sample diameters (500, 250, 150, 125 and 75 nm) were performed under nominal constant strain rates in an Agilent G200 nanoindenter and the SEMentor, a custom-built in situ instrument, comprising a scanning electron microscope and a dynamic contact module (Agilent) [24]. Compressions tests were performed under nominal strain-rate control, whereby the desired displacement rates were maintained through an internal feedback loop between a voice coil applying a force and a capacitive plate measuring the resulting displacement. Displacements rates were prescribed through the following equation for a desired strain rate: $\dot{u} = \dot{\varepsilon} l_0$ where l_0 is the initial pillar length. Actual displacement rates were then measured through the slope of the displacement vs. time data for the nearly elastic loading sections as seen in Fig. 2. The displacement rates ranged from ~0.15 to $\sim 700\ \mathrm{nm\ s^{-1}}$. While sub-nanometer displacement rates may seem spurious, the feedback loop was able to perform tests at these very slow speeds. Fig. 2A and B show the displacement and force vs. time for two $D \sim 125$ nm compression tests. The average displacement rates in Fig. 2A and B were measured to be ~0.37 and $194\ \mathrm{nm\ s^{-1}}$, respectively. This displacement rate is relatively constant throughout the test, apart from characteristic displacement bursts and the subsequent machine response required by the feedback loop. As the minimum aspect ratio of pillar compressions was chosen to be ~3:1 to minimize geometric constraints, there is a natural lower bound to the accessible strain rates. Tests at $\dot{u} < 0.1\ \mathrm{nm\ s^{-1}}$ were not attempted and are not expected to give reliable results. In this study, ~150 successful compression tests were performed, resulting in an average of ~5 compressions per data point in Fig. 5A. Details of the specific experimental attributes in performing nanoscale compression tests including rounding of the pillar tops, misalignment and geometric constraints are discussed in detail in Refs. [1,25,26].

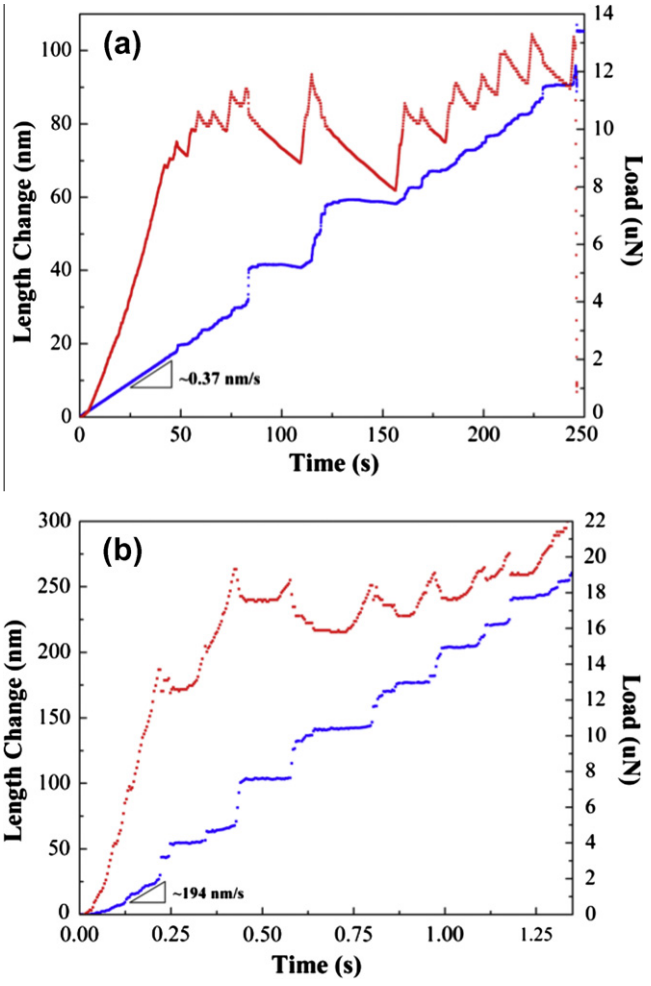

Fig. 2. Load (red) and length change (blue) vs. time for two $D \sim 125$ nm pillar compression tests. The measured displacement rates in *A* and *B* are 0.37 and $194\ \mathrm{nm\ s^{-1}}$, respectively, while nominally prescribed ones are 0.38 and $200\ \mathrm{nm\ s^{-1}}$, respectively. Displacement excursions correspond to load drops as a result of dislocation bursts. The constant-displacement sections are due to the feedback loop maintaining a constant average displacement rate. (For interpretation of the references to color in this figure legend, the reader is referred to the web version of this article.)

3. Results

3.1. Stress–strain behavior

Characteristic stress–strain curves are shown in Fig. 3: the four different stress–strain curves correspond to two

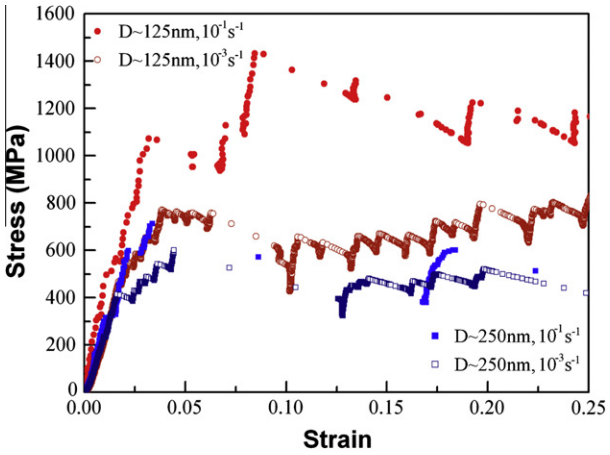

Fig. 3. Four characteristic stress–strain curves plotted for pillars of two different diameters, 125 and 250 nm, each deformed at two different strain rates, 10^{-3} and 10^{-1} s^{-1}. At a constant strain rate, smaller pillars have higher strengths, whereas at constant diameter, faster strain rates result in higher strengths. Plastic deformation continues beyond 25% strain, followed by unloading in all the compression tests above. Deformation behavior beyond 25% strain is omitted for clarity.

distinct diameters, 125 and 250 nm, each of which is deformed under two different strain rates, 10^{-1} and 10^{-3} s^{-1}. The stress plotted here is true stress following the analysis assuming a homogeneously deforming pillar while correcting for the elastic response of the pillar acting as an indenter into the substrate [3]. All of the stress–strain curves have a nearly elastic loading followed by intermittent strain bursts. It is noticeable that there is no appreciable global hardening across all pillars tested. In comparing the two different sizes at a constant strain rate, there exists a clear size effect, whereby smaller pillars exhibit strengths much greater than that of bulk. Furthermore, at a constant pillar diameter, faster strain rates result in higher stresses with the increase in strength significantly larger for smaller pillar diameters. Interestingly, increasing the strain rate by two orders of magnitude results in only a 15% strength increase in 250 nm pillars, while the strength in 125 nm pillars increases by almost 100% upon the same strain-rate increase, suggesting an increased strain-rate sensitivity in smaller pillars (Fig. 5A). It also appears that the faster strain-rate compressions result in one catastrophic strain burst as opposed to the multiple successive bursts characteristic of the slower strain rates (Fig. 3).

3.2. Size-dependent strength

Fig. 4a shows a log–log plot of flow stress at 10% strain as a function of pillar diameter for five different pillar diameters between 75 and 500 nm deformed at three different constant strain rates: from 10^{-1} to 10^{-3} s^{-1}. If a strain burst occurs at 10%, the strain at the last point in the previous loading region is chosen as the recorded stress. Stresses are not recorded for values inside a burst because as the pillar is deforming the machine is also removing load in order to maintain a constant displacement rate. The two combined effects result in an unclear instantaneous stress level during a burst. This plot reveals that pillars with larger diameters, i.e. 150–500 nm, obey the widely observed power-law size effect for all strain rates tested, with a power-law slope of ~0.54, well within the previously reported range [1]. Across three different strain rates, the power-law slope remains nearly constant despite a noticeable increase in strength with increasing strain rate. This suggests that the power-law slope in this size regime is not significantly affected by strain rate, and therefore by thermal contributions. The results for the fastest strain rate of 10^{-1} s^{-1} show this continuous power-law behavior extending down to the smallest diameter tested, i.e. 75 nm. At the two slower strain rates, however, a transition diameter exists, below which the pillar strength deviates

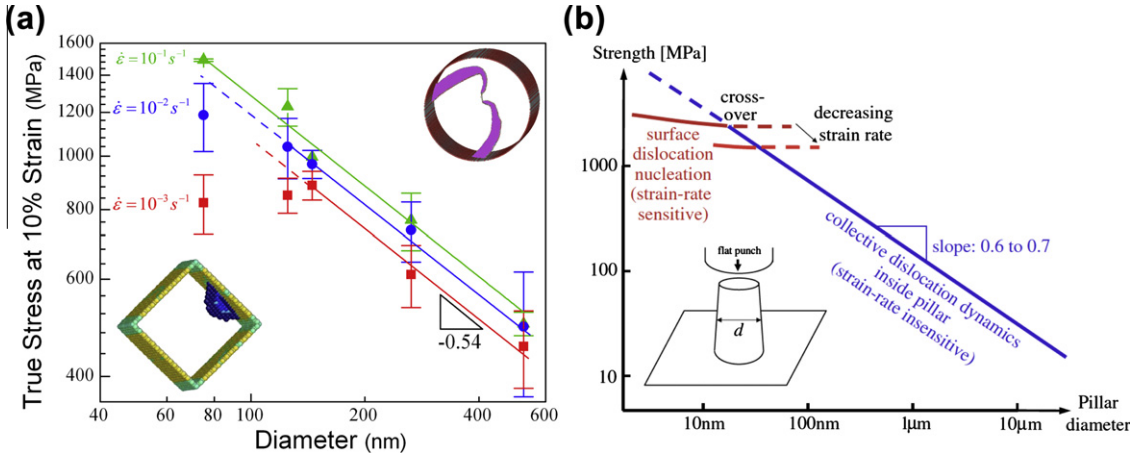

Fig. 4. (a) Strength as a function of diameter for three different strain rates (log–log scale). Trend lines denote power-law strengthening where plasticity is governed by collective DD. Inset shows atomistic simulation of two SASs sharing a pinning point [63]. At the transition diameter, specific to each strain rate, the mechanism changes to SS nucleation, as reflected in a deviation from the power-law strengthening. Bottom left inset shows atomistic simulations of a SS (reprinted with permission from APS) [20]. Top right inset depicts two single arm sources with one shared pinning point [63]. (b) Theoretical predictions by Zhu et al. [20], showing a nearly identical trend (reprinted with permission from APS).

from the power-law trend (indicated by a dashed line). This transition diameter, or the smallest diameter unambiguously continuing the power-law trend, is not constant and appears to decrease with increasing strain rate: $D_t \sim 150$ nm for 10^{-3} s^{-1}; $D_t \sim 125$ nm for 10^{-3} s^{-1}; and $D_t \sim \leqslant 75$ nm for 10^{-2} s^{-1}. Precise identification of the transition diameter is challenging; however, there is a clear trend that faster strain rates result in smaller transition diameters.

3.3. Strain-rate sensitivity and activation volume

A material's strain-rate dependence is usually quantified through an empirical fit of $\sigma = \sigma_0 \dot{\varepsilon}^m$ where m is the commonly reported strain-rate sensitivity. The strain-rate dependence, indicative of the rate-controlling mechanism, for dislocation source operation can also be described by an Arrhenius form that connects the shear strain rate, $\dot{\gamma}$, to the applied shear stress, τ [21]:

$$\dot{\gamma} = \dot{\gamma}_0 \exp\left(-\frac{Q^* - \tau\Omega(\tau, T)}{k_B T}\right) \quad (1)$$

where $\dot{\gamma}_0$ is a constant related to the source's attempt frequency, Q^* is the activation energy, k_B is Boltzmann's constant, and T is the temperature. The activation volume expressed above describes how the activation free energy changes with shear stress or $\Omega(\tau, T) \equiv -\frac{\partial Q}{\partial \tau}\big|_T$, and thus can be used to determine the activation volumes in nanopillar compression experiments through conducting tests at different constant strain rates [7]. Specifically Eq. (1) can be rewritten to show that [21]:

$$\Omega = k_B T \frac{\partial \ln(\dot{\gamma})}{\partial \tau} \quad (2)$$

We determined the strain-rate sensitivity and activation volumes for all of our compression tests at different strain rates, spanning over three orders of magnitude. The experimental data for the flow stress at 10% strain as a function of strain rate for five different diameters is shown on a log–log plot in Fig. 5A. In Fig. 5A, the slopes of the curves correspond to the strain-rate sensitivity, m. It is noteworthy that at high strain rates $\dot{\varepsilon} \geqslant 10^{-1}$ s^{-1}, corresponding to power-law behavior for all diameters tested (Fig. 4A), all pillar diameters show an increasing rate dependence with decreasing diameter, with m ranging between ~0.027 and ~0.057; these values are all >5-fold greater than that of bulk single-crystalline Cu (~0.006) [27]. This finding suggests that as the size is reduced, not only does the strength increase, but the strain-rate dependence of fcc materials emerges and increases as well. Furthermore, at intermediate strain rates $\dot{\varepsilon} < 10^{-2}$ s^{-1}, the two smallest diameters, 75 and 125 nm, show a discrete transition to a much stronger rate dependence, ~0.11, than the m at the three larger diameters, 0.027–0.04, suggesting a transition to a different deformation mechanism. The precise choice of transition strain rate is difficult to determine due to the inherent stochastic response of these compression tests. A first approximation of the transition strain rate for a given diameter was estimated from Fig. 4A. Subsequently, best fits of the stress vs. strain rate data were determined as common mechanisms are assumed to maintain similar trends in both strength and strain-rate sensitivity with size.

It may be possible to gain insights into the microstructural plasticity mechanisms responsible for this surprising strain-rate sensitivity by analyzing the activation volume. The experimental results of the activation volume, along with error bars corresponding to the accuracy of the fit, for each diameter at high strain rates, $\dot{\varepsilon} \geqslant 10^{-1}$ s^{-1} are

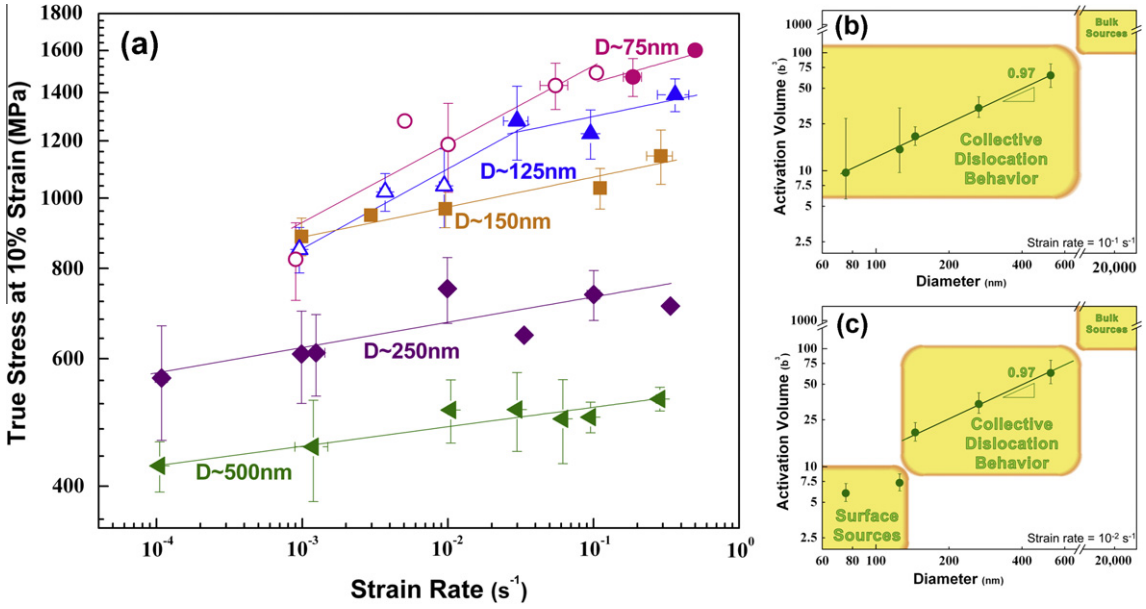

Fig. 5. (a) Flow stress at 10% strain as a function of strain rate for five different pillar diameters shown around each data set. The extracted activation volumes for each diameter at strain rates of (b) 10^{-1} s^{-1} and (c) 10^{-2} s^{-1}. These activation volumes may correspond to two distinct plasticity mechanisms: surface dislocation nucleation vs. collective DD.

plotted in Fig. 5B. This plot reveals a trend of smaller pillars having smaller activation volumes. The best fit of the activation volume as a function of pillar diameter data on a log–log plot has a nearly linear slope of ~0.97, implying that the Ω scales linearly with pillar diameter D. Notably, the activation volume here lies between $9.6b^3$ and $62b^3$, a range that is larger than that predicted for SS operation with the exception of the 75 nm diameter pillars. The large error bars for the two smallest diameters in Fig. 5C correspond to the limited range of strain rates over which this regime was experimentally measured. Fig. 5C shows a similar plot for the activation volume at slower strain rates, $\dot{\varepsilon} \leqslant 10^{-2}$ s^{-1}, and illustrates that the two smallest diameters have activation volumes of $\sim 6b^3$ and $\sim 7.3b^3$, respectively, approximately 50% and 40% smaller than the activation volumes at faster strain rates, with the magnitudes expected for SS nucleation: $1–10b^3$ [20]. The range of activation volumes expected for conventional bulk sources is plotted for comparison and completeness [7].

4. Discussion

4.1. Influence of sample fabrication on mechanical properties

To date, the vast majority of experiments on fcc nanopillars have been performed on samples fabricated by the use of the FIB [1]. Pillars fabricated via this methodology exhibit size-dependent strengths, and the mechanisms responsible for this strengthening have been a heavily debated topic [1]. One of the major points of contention has been the influence of the FIB fabrication technique on nanopillar strength [3,10,23,28–38] as the FIB introduces damage into the surface of the pillar by forming dislocation loops and surface amorphization [37]. Damage of this type is a known source of strengthening in bulk single crystals, suggesting that FIB-fabricated pillars may be stronger than bulk [37]. Thus, as the relative surface area to volume ratio in pillars increases with decreasing pillar diameter, these ion damage effects become more adverse. Further studies of the effects of the FIB damage and dislocation structure evolution through Laue microdiffraction [32–36,39], X-ray microdiffraction [31,38] and in situ TEM [40] have provided valuable insight into the role FIB-induced microstructural damage plays in a pillar's mechanical response.

Several initial investigations of pillars produced without the FIB have produced pristine uniaxial samples that deform in tension and compression at near-theoretical strength [28,29,41]; however, it has been shown that initially pristine Mo–Al–Ni eutectic alloys undergo a significant decrease in strength after exposure to the FIB or pre-strain as a result of increasing damage/dislocation density [30]. Effects of pre-strain are not limited to this system and in fact have been observed in fcc Au [42].

Among others, the current authors have recently shown that it is the initial dislocation density rather than the fabrication technique that drives the size effect in fcc metals [10,17,23,42,43]. In those experiments, similar arrays of Cu nanopillars as those used here were produced via electron beam lithography and electroplating. These pillars as fabricated contained initial dislocation densities of $\sim 10^{14}$ m^{-2} [23]. These dislocation densities are at the high end of the range of dislocation densities reported in FIB-fabricated fcc pillars: 10^{12} and 10^{14} m^{-2} [17,23,42,44]. Examples of these electroplated pillars are shown in Fig. 1B and C. These pillars, which have never been exposed to a FIB, demonstrate an identical size-dependent strengthening trend as found for all FIB-produced fcc pillars with similar initial dislocation densities [23]. This finding is consistent with previous work on bcc alloy systems, showing that the pillar strength is a strong function of the initial dislocation density. A key finding here is that as a result of similar relationships between strength and diameter, we expect the observed trends here to apply to FIB-fabricated fcc pillars; however, at the moment, fabrication limitations make producing sufficiently small pillars within the transition size range overly cumbersome. We also note that while there have been several investigations into the effects of FIB on the previously reported size-dependent regime, we know of no investigations into how FIB damage may enhance or diminish the observed transition seen here.

4.2. Nanoscale crystalline plasticity: dislocation starvation

A characteristic feature of the plastic deformation in pillars with non-zero initial dislocation densities is the stochastic nature of the intermittent strain bursts, corresponding to discrete dislocation avalanches [45–47]. In large systems, these avalanches are the result of collective dislocation motion; however, as pillar diameters decrease to the deep sub-micron regime, dislocation sources will be required to sustain plastic deformation, as dislocations will more readily annihilate at a free surface, as seen in both in situ [40] and post-deformation TEM [23], without forming extensive dislocation networks. For example, in a 300 nm tall pillar, 10% of nominal axial plastic strain in a ⟨1 1 1⟩-oriented Cu pillar would require ~125 dislocations to reach the free surface in order to carry that plastic strain. In the materials tested here, a 100 nm diameter pillar has an estimated initial dislocation density of $\sim 10^{14}$ m^{-2}, corresponding to only a few dislocations initially residing within the pillar. For instance, in a 100 nm diameter pillar, a single 2 nm dislocation would result in a dislocation density of $\sim 10^{12}$ m^{-2}, whereas a dislocation extending the diameter would result in a dislocation density of $\sim 10^{14}$ m^{-2}. This suggests that in these small diameter pillars dislocation avalanches must experience an increasing contribution from simultaneous operation of different sources, as the initial dislocation density is far from sufficient to carry the required plastic strain.

The increasing influence of source operation in these small pillars does not suggest that the dislocation density will vanish after appreciable plastic strain. These pillars are ~⟨1 1 1⟩ oriented, resulting in one ⟨1 1 1⟩ slip plane normal to the loading direction thus having no resolved

shear stress on that plane. Post-deformation TEM studies on these pillars show that within the deforming region, only dislocations lying in this slip plane remain in the pillar, resulting in a non-zero dislocation density [23].

4.3. Choice of 10% flow stress and impact on activation volume

We chose to report flow stress at 10% strain because in these small samples the determination of yield point is ambiguous and, for the Cu pillars tested here, there is, in general, no global hardening in the stress–strain response as illustrated in Fig. 3. This lack of global hardening outside the initial plastic region has also been observed in other FIB-fabricated Cu pillars [48] and suggests that beyond the initial plastic deformation as high as 10% strain, the choice of strain to report flow stress does not affect the power-law slope or the reported strain-rate sensitivity. Furthermore, one of the consequences of dislocation starvation is that the internal microstructure should not appreciably change as a function of strain, allowing the use of the flow stress at 10% strain in estimates of activation volume for either SSs or SASs. In contrast, in samples or sizes where dislocation substructures evolve with strain, the deformation mechanisms will evolve with strain, and the choice of characteristic flow stress should be carefully considered.

4.4. Surface source strength and activation volume

While transitions from power-law behavior in fcc metals have not been investigated experimentally, they were recently predicted using a combination of analytical and atomistic theory by Zhu et al. [20]. These authors raised the question of what would happen if SSs were the dominant mechanism in small volume plasticity [20]. Following their analysis, the nucleation frequency of a surface dislocation source due to an applied stress can be described by Eq. (1), where the nucleation frequency corresponds to the resulting shear strain rate of Eq. (1). In order to describe the stress for nucleating a dislocation burst, they define a survival probability $f(t)$, which describes the percentage of pillars that have not nucleated a dislocation burst by a time t. The change in the survival probability with time can then be described by:

$$\frac{\partial f(t)}{\partial t} = -\nu f(t) \tag{3}$$

where ν is the nucleation frequency. This function can be rewritten in terms of uniaxial stress through a linear elastic relation: $\sigma = E\dot{\varepsilon}t$ as pillar compressions show nearly elastic loading between bursts. In order to find the most probable stress at which a pillar will nucleate a burst, we look for the maximum in the change of the survival probability. The resulting predicted stress can be written most clearly through a linearized form of the stress dependence:

$$\sigma = \sigma_a - \frac{k_B T}{\Omega} \ln \frac{k_B T N \nu_0}{E\dot{\varepsilon}\Omega} \tag{4}$$

The likely stress for nucleating a dislocation from a SS is then related to two components: the athermal strength, σ_a, and the last term on the right-hand side, describing the thermal contribution. Examining the latter term, the thermal contribution is proportional to $\frac{1}{\Omega}\ln\frac{1}{\Omega}$, showing that for mechanisms with smaller activation volumes, the thermal contribution plays a larger role. It should be noted that this analysis is general for any dislocation source. Furthermore, in the event of repeated successive bursts, the physics described above holds true as long as the microstructure does not change appreciably with strain. It should be noted that in micro-pillars dislocation substructures progressively develop and change with increasing strain, rendering the above analysis inapplicable to these larger samples. Deep in the sub-micron regime, however, dislocations do not readily form substructures, and therefore this analysis should be relevant at all strains.

The linearized form of the strength of a SS can be used to predict the diameter dependence of SS operation. Fig. 4B [20] shows a sketch of the theoretically predicted strength as a function of diameter on a log–log scale, which bears a strong resemblance to our experimental findings (Fig. 4A). Both of these plots convey that larger pillars strengthen in a power-law fashion whose slope is relatively independent of strain rate, or thermal contributions, suggesting that the power-law dependence is proportional to the athermal strength. However, as the diameter decreases, a competition between the power-law and SS-dominated plasticity arises, where the weaker of the two governs the overall response. Based on atomistic FENEB simulations, the activation volume for partial dislocation nucleation was found to be 1–10b^3, corresponding nucleation from a sharp corner, 1b^3, to an atomically smooth surface, 10b^3. Their atomistic predictions suggest a transition diameter in the range of 10–100 nm, depending on strain rate [20]. This predicted diameter range and strain-rate sensitivity of the transition diameter overlap favorably with our experimental results suggesting that in sufficiently small samples, surface nucleation of dislocations may be the dominant plasticity mechanism. This transition to partial dislocation nucleation has also been observed in tensile tests of Cu thin films and single-crystal Au, illustrating that similar mechanisms govern plasticity in all small-scale crystalline samples, irrespective of the sample geometry [2,54,55].

In order for the reasonable agreement found in Fig. 4 in both trend and magnitude between our experimental data and this atomistic work, the experimental results and atomistic simulations must reflect similar values in both the athermal strength and activation volume. The agreement in the activation volume has been shown above, suggesting these similarities likely hold true in at least the limited region accessed by our experiments. This further suggests that SSs are controlling the deformation of the smallest pillars tested at the slowest strain rates.

4.5. Size-dependent strength and transition diameter

Previous compression tests on similarly produced electroplated pillars have resulted in a size dependence with a power-law exponent of ~0.63 [23], similar to the ~0.54 reported here. Note that the previous compression tests were all conducted at a constant displacement rate of 2 nm s^{-1} as opposed to a constant strain rate as done here. The aspect ratio in both sets of experiments corresponds to a ~3:1 height to diameter, resulting in an increasing strain rate with decreasing pillar diameter, and therefore height, in tests performed at constant displacement rates. As a result, the ~0.63 exponent is, in fact, artificially high in relation to constant strain-rate tests. Correcting for the changing strain rate during these tests would bring the two power-law slopes into an even closer agreement.

The observed deviation from power-law strengthening at sub-micron pillar diameters has not been experimentally observed before since most experiments to date have been performed on larger pillars and/or not at constant strain rates [1,3,4,23,24,45,47,49–51]. This finding emphasizes the non-trivial role strain rate plays in the determination of the strength, a factor not yet systematically evaluated in fcc nanopillar experiments. Interestingly, Uchic et al. [4] reported a transition in power-law exponent for several micron-sized Ni_3Al–Ta pillars and speculated that the source to be the self-exhaustion or annihilation of screw dislocations.

The lack of strain-rate effect on the power-law slope demonstrates that the mechanism responsible for the power law is itself insensitive to strain rate, as the strain-rate dependence manifests itself as a deviation from the power law. In order to understand the strain-rate dependence of the power-law behavior, we examine a useful form for small-scale crystalline strength [43,44,50]:

$$\sigma = \sigma_o + \frac{1}{2}\mu b\sqrt{\rho} + \frac{\alpha\mu b}{L}\ln\frac{L}{b} \tag{5}$$

where the first term on the right-hand side corresponds to friction stress, the second term is due to back-stresses from dislocation–dislocation interactions, and the last term originates from the SAS strength, where α is a constant prefactor corresponding to the character of the dislocation line [52]. Note that none of the terms above are expected to be strain-rate dependent. However, we also note that the above equation only takes into account athermal effects, rendering its ability to describe the thermally activated processes discussed here inadequate. As mentioned previously, Zhu's analysis is general for any dislocation source. If we apply Zhu's analysis [20] to understand the thermally activated nature of SASs, we notice that the athermal strength (the first term in Eq. (4)) corresponds to Eq. (5). The remaining term in Eq. (4), the thermal contribution, is proportional to $\frac{1}{\Omega}\ln\frac{1}{\dot{\varepsilon}\Omega}$. We have shown here that the measured activation volume is almost linear with diameter, suggesting that the thermal contribution would be proportional to $\frac{1}{D}\ln\frac{1}{\dot{\varepsilon}D}$. If the source length, L, in Eq. (5) and the pillar diameter, D, are linearly related, then both the thermal and athermal components of a SAS would have nearly the same size-dependent behavior as their size dependencies would be dominated by the pre-logarithm $1/D$ dependence. This added thermal contribution to Eq. (5) would not substantially change the observed power-law slope, which reflects the diameter dependence of the power-law seen in Fig. 4A. Furthermore, the addition of the thermal contribution would include the correct trend in the strain-rate dependence: a decrease in the strain rate rigidly shifts the power law to lower stresses. We note that the expected source length for a pillar is not precisely linear with its diameter; rather it will be a function of the dislocation density [43]. Furthermore in order to truly account for the thermal contributions in the mechanisms of nanopillars within the power-law regime, both atomistic and DD simulations would be required to accurately capture the correct physics and the relevant length scales and time scales.

4.6. Activation parameters

The range of strain rates explored in our experiments corresponds to a relatively narrow range of activation energies. The activation energy available to any mechanism is $Q = Mk_BT$, where M is of the order of the logarithm of the total number of atomic vibrations during a test. In our experiments, this gives M ranging from ~37 down to ~28 based on strain rates of $\sim 10^{-4}$–1 s^{-1}, and corresponds to a limited accessible energy range of ~0.95 eV down to ~0.72 eV [7,53]. All of the activation volumes we computed correspond to this relatively narrow energy range. Further exploration of the details of the activation energy vs. applied stress would require atomistic simulations and further experiments, including those over a range of constant temperature.

4.7. Expected trends in SAS activation volume

In order to determine whether the observed nearly linear trend in the SAS activation volume vs. diameter at fast strain rates, $\dot{\varepsilon} \geqslant 10^{-1}$ s^{-1}, is reasonable, we developed a simple phenomenological model that assumes the main change in activation volume with pillar diameter stems from SAS operation. This assumption is based on the idea that the length of a SAS is a strong function of the pillar diameter, whereas other collective dislocation behavior is to expected here to be independent of sample diameter. This phenomenological model approximates a SAS as ½ a FRS, shown schematically in Fig. 6A. In this case, the activation volume and energy of a SAS would correspond to those of ½ a FRS.

Following Nabarro's derivation for the activation volume of a FRS [53], there are two components to the activation volume. The first corresponds to the classical description of the activation volume of a bowing dislocation segment between two perfectly immobile pinning points. The second component accounts for the finite

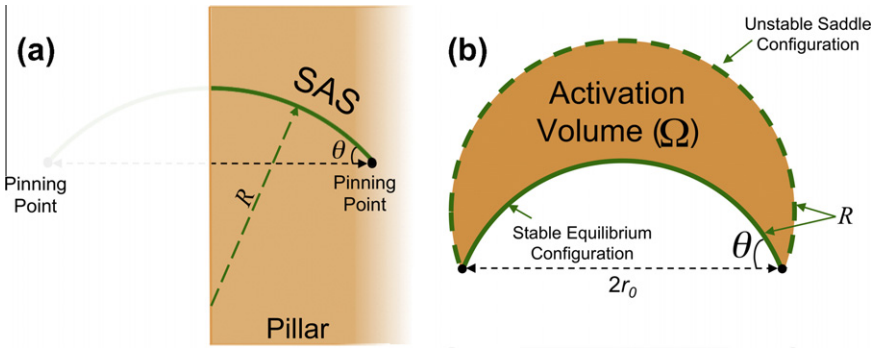

Fig. 6. (a) A schematic of a SAS represented as ½ a FRS. (b) The activation volume is determined as ½ the difference between the stable and unstable equilibrium configurations for a FRS at a particular applied stress.

strength, and thus the motion, of these pinning points. This latter component was introduced in order to reconcile the Cottrell–Stokes law with FRS operation [53]. The required strength for a SAS to multiply dislocations and thus govern plasticity in nanopillars is determined by the motion of a SAS around its stationary pinning point [52]. While simulations and experiments have shown that SASs are not immortal [9,17,56], the strength of a pinning point is not expected to be a strong function of the pillar diameter especially in large pillar diameters, but rather of its proximity to the free surface. However, the length of a SAS is a strong function of diameter, thus in our attempt to capture the trend in activation volume we focus here only on the contribution from the bowing of a dislocation line between two infinitely strong pinning points.

At a given applied shear stress, a dislocation segment pinned by two immobile pinning points has two equilibrium positions corresponding to the same radius of curvature, as schematically shown in Fig. 6B. In order for a FRS to produce a new dislocation, a certain amount of thermal energy is required to move the dislocation segment between the stable and unstable equilibrium positions. The activation volume is then defined as the geometry of the volume difference between these two configurations:

$$\Omega(\tau, r_0) = b(A^* - A_i) = b(\pi R^2 - 2A_i) \tag{6}$$

Generally, dislocation multiplication from a FRS is an athermal process, where the thermal component represents less than ~0.1% of the athermal strength for typical line lengths [53,57]. As a result, the distance between the two equilibrium positions is very small. Eq. (6) can then be simplified by rewriting the geometry of the dislocation segment in terms of the stress necessary to bow the dislocation segment through an angle θ: $\tau = \frac{\mu b \sin\theta}{2r_0}$ and the athermal strength of a FRS: $\tau_{ath} = \frac{\mu b}{2r_0}$ [58]. In the limit where τ is close to τ_{ath} and taking the dominant term, the resulting activation volume is approximately:

$$\Omega(\tau, r_0) \approx b r_0^2 \sqrt{\frac{2}{\tau_{ath}}(\tau_{ath} - \tau)} \tag{7}$$

The activation energy is then the integration of the parabolic dependence between source strength and activation volume in the region of athermal strength [59,60]: $Q \approx \frac{2}{3}(\tau_{ath} - \tau)\Omega$ and fixed in the narrow range described previously. We thus arrive at the following approximate scaling of the activation volume of SAS with its athermal strength: $\Omega \propto \tau_{ath}^{-5/3}$.

Fig. 4A shows that in the range of power-law strengthening for different strain rates, the absolute pillar strength increases with strain rate; however, the power-law exponent remains relatively insensitive to the strain rate. This suggests that the trend in athermal strength with diameter reflects the commonly reported power law. As a result, we write the activation volume as a function of diameter as $\Omega \propto D^{-5n/3}$. Comparing the diameter dependence of the activation volume to the experimental data presented here, we find that $\Omega \propto D^{0.9}$, close to the experimentally obtained exponent of 0.97. To date, fcc microcompression tests have a range of reported values for n, with the majority between 0.5 and 0.7, resulting in a range of possible exponents, 0.83–1.16, relating the activation volume to the pillar diameter. Despite the simplicity of this model, the combination of our experimental findings and those predicted by the model indicates that SASs strongly contribute to the size dependence of part of the strength in larger, micron-sized pillars. It should be noted that while this phenomenological model captures the relative trend, it does not accurately predict the magnitude of the observed activation volumes. The activation volumes suggested by this simple model are in the range of $\Omega > 400b^3$, which, as expected, reflect values for FRS operation. The lack of agreement in the magnitude of the activation volume shows that while this simple model reflects the dependence of the activation volume on diameter, there remain important open questions as to the other sources of thermal activation in fcc nanopillars and the applicability of classical theories such as Nabarro's to small-scale plasticity.

It should be noted that the above model does not take into account the image force or any extra thermal contribution from the nearby free surface. Simulations have shown that the effects of the image stress are negligible for the sources longer than ~250b, implying that the image force effects may only come to play a role in the smallest diameter pillars: $D \sim 75$ nm [61,62]. Furthermore, the

complete athermal strength of a SAS has a logarithmic dependence on the dislocation source length, i.e. the third term of Eq. (5), which—while a much smaller contribution than the inverse source length dependence—may account for some discrepancy between the experimental results and the model [2,8,54,55,61,62]. Also, as noted by Nabarro, the motion of the pinning points may contribute substantially to the thermal activation of a double-pinned source [53]. An alternate approach to determine the expected dependence of the activation volume with diameter would be to examine the expected source length with varying pillar diameter. This was done analytically by Rao et al. [61]; however, that model implicitly requires the knowledge of the dislocation density and distribution at each pillar diameter, which is unknown here [43]. The approach taken above subsumes all of the information regarding the dislocation density and distribution into the diameter dependence on strength, which we suggest is proportional to the observed power law.

5. Summary

We demonstrate a notable effect of both strain rate and sample size on the compressive strength of single-crystalline Cu nanostructures. By determining the activation volume for each pillar diameter and strain rate, we observe a clear transition in the slope of strength vs. strain rate for the two smallest diameters, 75 and 125 nm, while these slopes remain constant for larger pillars. Further, we report a deviation from the ubiquitously reported power-law size-dependent strength for the smallest pillar diameters and at the slowest strain rates, as predicted by theory. Based on our experimental findings, existing atomistic simulations and theory, we postulate that this strain-rate sensitivity arises from the operation of surface dislocation sources of a highly thermal nature. We believe that these findings may provide further insight into small-scale plasticity and facilitate the elucidation of the full extent of size effects, as well as the corresponding governing deformation mechanisms.

Acknowledgements

The authors gratefully acknowledge Wei Cai, Chris Weinberger and Ting Zhu for useful discussions. Further, we would like to thank Wei Cai and Chris Weinberger for the SAS atomistic image. A.T.J., J.L. and J.R.G. gratefully acknowledge the financial support of the National Science Foundation through A.T.J.'s NSF Graduate Research Fellowship, J.L.'s NSF CMMI-0728069 and J.R.G.'s CAREER Grant DMR-0748267.

References

[1] Uchic MD, Shade PA, Dimiduk DM. Ann Rev Mater Res 2009;39:361.
[2] Kraft O, Gruber P, Mönig R, Weygand D. Ann Rev Mater Res 2010;40:293.
[3] Greer JR, Oliver WC, Nix WD. Acta Mater 2005;53:1821.
[4] Uchic MD, Dimiduk DM, Florando JN, Nix WD. Science 2004;305:986.
[5] Volkert CA, Lilleodden ET. Philos Mag 2006;86:5567.
[6] Courtney TH. Mechanical behavior of materials. Long Grove: Waveland Press; 2000.
[7] Zhu T, Li J. Prog Mater Sci 2010;55:710.
[8] Weinberger CR, Cai W. PNAS 2008;105:14304.
[9] Tang H, Schwarz KW, Espinosa HD. Acta Mater 2007;55:1607.
[10] El-Awady JA, Woodward C, Dimiduk DM, Ghoniem NM. Phys Rev B 2009;80:104104.
[11] Guruprasad PJ, Benzerga AA. J Mech Phys Solids 2008;56:132.
[12] Balint DS, Deshpande VS, Needleman A, Van der Giessen E. Model Simul Mater Sci Eng 2006;14:409.
[13] Rao SI, Dimiduk DM, Parthasarathy TA, Uchic MD, Tang M, Woodward C. Acta Mater 2008;56:3245.
[14] Diao JK, Gall K, Dunn ML, Zimmerman JA. Acta Mater 2006;54:643.
[15] Park HS, Gall K, Zimmerman JA. J Mech Phys Solids 2006;54:1862.
[16] Gall K, Diao JK, Dunn ML. Nano Lett 2004;4:2431.
[17] Oh SH, Legros M, Kiener D, Dehm G. Nat Mater 2009;8:95.
[18] Zheng H, Cao A, Weinberger C, Huang J. Nature 2010.
[19] Lu Y, Huang JY, Wang C, Sun SH, Lou J. Nat Nanotechnol 2010;5:218.
[20] Zhu T, Li J, Samanta A, Leach A, Gall K. Phys Rev Lett 2008;100:025502.
[21] Krausz AS, Eyring H. Deformation kinetics. New York: John Wiley; 1975.
[22] Burek MJ, Greer JR. Nano Lett 2010;10:69.
[23] Jennings AT, Burek MJ, Greer JR. Phys Rev Lett 2010;104:135503.
[24] Kim JY, Greer JR. Acta Mater 2009;57:5245.
[25] Greer JR, Jang DC, Kim JY, Burek MJ. Adv Funct Mater 2009;19:2880.
[26] Greer JR, Kim JY, Burek MJ. JOM 2009;61:19.
[27] Chen J, Lu L, Lu K. Scripta Mater 2006;54:1913.
[28] Bei H, Shim S, George EP, Miller MK, Herbert EG, Pharr GM. Scripta Mater 2007;57:397.
[29] Richter G, Hillerich K, Gianola DS, Mónig R, Kraft O, Volkert CA. Nano Lett 2009;9:3048.
[30] Shim S, Bei H, Miller MK, Pharr GM, George EP. Acta Mater 2009;57:503.
[31] Maass R, Grolimund D, Van Petegem S, Willimann M, Jensen M, Van Swygenhoven H, et al. Appl Phys Lett 2006;89:151905.
[32] Maass R, Van Petegem S, Borca C, Van Swygenhoven H. Mater Sci Eng A 2009;524:40.
[33] Maass R, Van Petegem S, Grolimund D, Van Swygenhoven H, Kiener D, Dehm G. Appl Phys Lett 2008;92:071905.
[34] Maass R, Van Petegem S, Ma D, Zimmermann J, Grolimund D, Roters F, et al. Acta Mater 2009;57:5996.
[35] Maass R, Van Petegem S, Van Swygenhoven H, Derlet PM, Volkert CA, Grolimund D. Phys Rev Lett 2007;99:145505.
[36] Maass R, Van Petegem S, Zimmermann J, Borca CN, Van Swygenhoven H. Scripta Mater 2008;59:471.
[37] Kiener D, Motz C, Rester M, Jenko M, Dehm G. Mater Sci Eng A 2007;459:262.
[38] Budiman AS, Han SM, Greer JR, Tamura N, Patel JR, Nix WD. Acta Mater 2008;56:602.
[39] Kirchlechner C, Kiener D, Motz C, Labat S, Vaxelaire N, Perroud O, et al. Philos Mag 2011;91:1256.
[40] Shan ZW, Mishra RK, Syed Asif SA, Warren OL, Minor AM. Nat Mater 2008;7:115.
[41] Brenner SS. J Appl Phys 1956;27:1484.
[42] Lee SW, Han SM, Nix WD. Acta Mater 2009;57:4404.
[43] Parthasarathy TA, Rao SI, Dimiduk DM, Uchic MD, Trinkle DR. Scripta Mater 2007;56:313.
[44] Norfleet DM, Dimiduk DM, Polasik SJ, Uchic MD, Mills MJ. Acta Mater 2008;56:2988.
[45] Ng KS, Ngan AHW. Acta Mater 2008;56:1712.

[46] Csikor FF, Motz C, Weygand D, Zaiser M, Zapperi S. Science 2007;318:251.
[47] Brinckmann S, Kim J-Y, Greer JR. Phys Rev Lett 2008;100:155502.
[48] Kiener D, Minor AM. Acta Mater 2011;59:1328.
[49] Kiener D, Grosinger W, Dehm G. Scripta Mater 2009;60:148.
[50] Dimiduk DM, Uchic MD, Parthasarathy TA. Acta Mater 2005;53:4065.
[51] Kiener D, Motz C, Schöberl T, Jenko M, Dehm G. Adv Eng Mater 2006;8:1119.
[52] Hirth JP, Lothe J. Theory of dislocations. New York: John Wiley; 1982.
[53] Nabarro FRN. Acta Metall Mater 1990;38:161.
[54] Gruber PA, Boehm J, Onuseit F, Wanner A, Spolenak R, Arzt E. Acta Mater 2008;56:2318.
[55] Gruber PA, Solenthaler C, Arzt E, Spolenak R. Acta Mater 2008;56:1876.
[56] Weinberger C. Scripta Mater 2010;64:529.
[57] Estrin Y, Kim HS, Nabarro FRN. Acta Mater 2007;55:6401.
[58] Hull D, Bacon DJ. Introduction to dislocations. Oxford: Elsevier; 2001.
[59] Christian JW, Masters BC. Proc Roy Soc Lond Ser A 1964;281:240.
[60] Shemensk Rm. ASM Trans Quart 1965;58:360.
[61] Rao S, Dimiduk D, Tang M, Parthasarathy T, Uchic M, Woodward C. Philos Mag 2007;87:4777.
[62] Pichaud B, Minari F, Kellerhals J. Philos Mag A 1978;38:593.
[63] Weinberger C, Cai W. Private communication.